Dirichlet-to-Neumann map method for analyzing periodic arrays of cylinders with oblique incident waves

Yumao Wu[1,2,3,*] and Ya Yan Lu[3]

[1] *Joint Advanced Research Center of University of Science and Technology of China and City University of Hong Kong, Suzhou, Jiangsu, China*

[2] *Department of Mathematics, University of Science and Technology of China Hefei, Anhui, China*

[3] *Department of Mathematics, City University of Hong Kong, Kowloon, Hong Kong*

[*] *Corresponding author: ymwu@mail.ustc.edu.cn*

For finite two-dimensional (2D) photonic crystals given as periodic arrays of circular cylinders in a square or triangular lattice, we develop an efficient method to compute the transmission and reflection spectra for oblique incident plane waves. The method relies on vector cylindrical wave expansions to approximate the Dirichlet-to-Neumann (DtN) map for each distinct unit cell, and uses the DtN maps to derive an efficient method that works on the edges of the unit cells only. The DtN operator maps the two longitudinal field components to their derivatives on the boundary of the unit cell.

OCIS codes: 050.5298,000.4430

1. Introduction

Due to their unprecedented ability to control and manipulate light, photonic crystals (PhCs) have emerged as an important class of optical materials [1]. Along with the rapid progress in nano-fabrication techniques, there is a need to improve numerical simulation techniques to further speed up the design and optimization of PhC structures and devices. Mathematical problems associated with PhCs include eigenvalue problems for band structures, PhC waveguide and microcavity modes, and boundary value problems for finite PhCs, PhC devices involving many defect unit cells and other hybrid structures. Over the years, many numerical methods have been developed for analyzing PhC structures and devices. Some of these are general methods, such as the finite-difference time-domain (FDTD) method [2], that

can be used to study various aspects of PhCs, while other methods are specially designed for a restricted class of problems. The special methods usually exploit some available geometry features of the PhC structures. For example, since PhC devices are usually fabricated using a small number of different materials, the boundary integral equation method [3, 4] formulated on the material interfaces often outperform the more general finite element method. Meanwhile, since many PhCs are designed using circular rods or air-holes, the multipole method [5–7] based on cylindrical wave expansions often have significant advantages compared with other methods. Partial periodicity in PhC devices can also be taken advantage of by Bloch mode expansion and recursive-doubling techniques used in the scattering matrix formalism [8, 9].

In previous work, we developed the so-called Dirichlet-to-Neumann (DtN) map method to take advantage of the underlying lattice structure and the existence of many identical unit cells in a typical PhC structure or device. The main idea is to calculate an operator (the DtN map, to be approximated by a matrix) for each unit cell, so that further computation does not involve its interior. The method has been used to analyze band structures [10, 11], PhC waveguides [12], microcavities [13], transmission and reflection spectra of finite PhCs [14–16], and general PhC devices involving waveguides that extend to infinity [17]. To construct the DtN map for a unit cell, we use either cylindrical wave expansions or boundary integral equations [18].

The DtN map technique developed in previous work is limited to ideal 2D problems where both the structure and the wave fields are invariant in a direction, say z. For linear and isotropic media, this leads to scalar 2D problems involving the E and H polarizations separately. In this paper, we extend the DtN map technique to out-of-plane propagation problems of ideal 2D PhC structures. More precisely, the structure is still invariant in z, but we assume that wave fields vary with z as $\exp(i\gamma_0 z)$, where γ_0 is the wave vector component in the z direction. Such a study is relevant for PhC fibers where z is the fiber axis [6], and it is a necessary step for analyzing 3D PhC woodpile structures where each layer is invariant in one direction [7]. We concentrate on 2D PhCs involving circular cylinders on a square or triangular lattice, and construct a DtN map based on vector cylindrical waves. Although the DtN map can be used in various problems, we only use it to calculate transmission and reflection spectra for finite PhCs, i.e., finite number of periodic arrays of cylinders.

The mathematical formulation is identical to that of diffraction gratings in conical mounting. Therefore, many existing numerical methods are available, including the classical modal method [19–21], the Fourier modal methods [22, 23], the differential method [24], the finite element method [25, 26], the integral equation method [27–30], the multipole method [6–9], etc. The classical and Fourier modal methods are suitable for layered structures and the accuracy is limited by the staircase approximation for the boundaries of the cylinders. The

differential method recasts the problem as a boundary value problem for a large system of ordinary differential equations which is relatively expensive to solve. The finite element method discretizes one period of the structure leading to large, sparse, complex, indefinite systems that are also expensive to solve. The integral equation method involves the quasi-periodic Green's function which requires sophisticated lattice sums techniques to evaluate. The multipole method is relatively efficient, but it also requires lattice sums. In the following, we show that the DtN map method is highly competitive in both accuracy and efficiency.

2. Problem formulation

2.A. Basic equations

We consider the scattering of a plane incident wave by an ideal two-dimensional (2D) structure whose relative permittivity (dielectric constant) ε and the relative magnetic permeability μ are functions of $\mathbf{r} = (x, y)$ only (i.e., independent of z), where $\{x, y, z\}$ forms a Cartesian coordinate system. If the incident plane wave depends on z as $\exp(i\gamma_0 z)$, where γ_0 is a real constant, then the scattered fields have the same z dependence, and the variable z can be completely separated. Under these conditions, we only need to work on the z components of the electric and magnetic fields: E_z and $\tilde{H}_z$, where $\tilde{\mathbf{H}} = \sqrt{\mu_0/\varepsilon_0}\mathbf{H}$ is the scaled magnetic field and $\tilde{H}_z$ is its z component, ε_0 and μ_0 are the permittivity and magnetic permeability of vacuum. From the frequency domain Maxwell's equations, it is easily seen that the other four components are given by

$$\begin{bmatrix} E_x \\ E_y \end{bmatrix} = \frac{i}{\eta}\left[\gamma_0 \nabla E_z + k_0 \mu \mathbf{J} \cdot \nabla \tilde{H}_z\right], \tag{1}$$

$$\begin{bmatrix} \tilde{H}_x \\ \tilde{H}_y \end{bmatrix} = \frac{i}{\eta}\left[\gamma_0 \nabla \tilde{H}_z - k_0 \varepsilon \mathbf{J} \cdot \nabla E_z\right], \tag{2}$$

where $k_0 = \omega/c$ is the free space wavenumber, c is the speed of light in vacuum, ω is the angular frequency, $\exp(-i\omega t)$ is the assumed time dependence, $\nabla = [\partial_x, \partial_y]^T$ is the 2D gradient operator, and

$$\eta = k_0^2 \varepsilon \mu - \gamma_0^2, \quad \mathbf{J} = \begin{bmatrix} 0 & 1 \\ -1 & 0 \end{bmatrix}.$$

Furthermore, the two z components satisfy the following system of equations

$$\nabla \cdot \left(\frac{\varepsilon}{\eta}\nabla E_z\right) + \nabla \cdot \left(\frac{\gamma_0}{k_0 \eta}\mathbf{J} \cdot \nabla \tilde{H}_z\right) + \varepsilon E_z = 0, \tag{3}$$

$$\nabla \cdot \left(\frac{\mu}{\eta}\nabla \tilde{H}_z\right) - \nabla \cdot \left(\frac{\gamma_0}{k_0 \eta}\mathbf{J} \cdot \nabla E_z\right) + \mu \tilde{H}_z = 0, \tag{4}$$

where $\nabla\cdot$ is the 2D divergence operator.

If the wave fields do not depend on z, i.e., $\gamma_0 = 0$, then equations (3) and (4) are reduced to two separate Helmholtz equations corresponding to the E and H polarizations:

$$\nabla \cdot \left(\frac{1}{\mu}\nabla E_z\right) + k_0^2 \varepsilon E_z = 0, \tag{5}$$

$$\nabla \cdot \left(\frac{1}{\varepsilon}\nabla \tilde{H}_z\right) + k_0^2 \mu \tilde{H}_z = 0. \tag{6}$$

In general, when $\gamma_0 \neq 0$, E_z and $\tilde{H}_z$ are coupled. However, in a homogeneous region where ε and μ (thus η) are constants, both equations (3) and (4) are reduced to

$$\Delta\phi + \eta\phi = 0, \tag{7}$$

where Δ is the 2D Laplacian and ϕ can be either E_z or $\tilde{H}_z$. If the structure has piecewise constant material parameters, then E_z and $\tilde{H}_z$ are only coupled on interfaces between different homogeneous media. Let Γ be a material interface, $\nu = (\nu_x, \nu_y)$ be a unit normal vector of Γ, $\tau = (-\nu_y, \nu_x)$ be the unit tangential vector of Γ, then E_z, $\tilde{H}_z$ and

$$\frac{\varepsilon}{\eta}\,\partial_\nu E_z + \frac{\gamma_0}{k_0\eta}\,\partial_\tau \tilde{H}_z, \quad \frac{\mu}{\eta}\,\partial_\nu \tilde{H}_z - \frac{\gamma_0}{k_0\eta}\,\partial_\tau E_z \tag{8}$$

must be continuous across Γ. Notice that in general the normal derivatives of E_z and $\tilde{H}_z$ are not continuous.

2.B. Diffraction of periodic structures

We are concerned with structures that are periodic in the x direction with a period L and finite in the y direction given by $0 < y < D$ for a constant D. For $y < 0$ (the bottom) and $y > D$ (the top), we have two homogeneous media with constant relative permittivity and permeability $\{\varepsilon_b, \mu_b\}$ and $\{\varepsilon_t, \mu_t\}$, respectively. In the top, we specify a plane incident wave with a wave vector $\mathbf{k}_0 = (\alpha_0, -\beta_0^{(t)}, \gamma_0)$ satisfying $\beta_0^{(t)} > 0$ and

$$\alpha_0^2 + [\beta_0^{(t)}]^2 = \eta_t = k_0^2 \varepsilon_t \mu_t - \gamma_0^2.$$

Let θ_0 be the angle between $\mathbf{k}_0$ and the z axis (the angle of conicity), and φ_0 be the angle between the projection of $\mathbf{k}_0$ on the xy plane and the x axis, we have

$$\alpha_0 = k_0\sqrt{\varepsilon_t\mu_t}\,\sin\theta_0\cos\varphi_0, \tag{9}$$

$$-\beta_0^{(t)} = k_0\sqrt{\varepsilon_t\mu_t}\,\sin\theta_0\sin\varphi_0, \tag{10}$$

$$\gamma_0 = k_0\sqrt{\varepsilon_t\mu_t}\,\cos\theta_0. \tag{11}$$

Notice that for $\beta_0^{(t)} > 0$, φ_0 must satisfy $180^o < \varphi_0 < 360^o$. The incident wave gives rise to the z-dependence $\exp(i\gamma_0 z)$ for all wave field components. To simplify the notation, we

suppress the z dependence and consider the wave fields as functions of $\mathbf{r} = (x, y)$. Therefore, the incident wave is

$$\mathbf{u}^{(i)}(\mathbf{r}) = \mathbf{A} \exp[i(\alpha_0 x - \beta_0^{(t)} y)], \quad y > D, \tag{12}$$

where $\mathbf{u} = [E_z, \tilde{H}_z]^T$, the superscript T denotes the transpose and $\mathbf{A}$ is a vector amplitude. The periodicity of the structure gives rise to the following quasi-periodic condition:

$$\mathbf{u}(x + L, y) = \exp(i\alpha_0 L)\, \mathbf{u}(x, y). \tag{13}$$

For $y > D$, we have a reflected wave $\mathbf{u}^{(r)}$, so that the total wave field is given by $\mathbf{u} = \mathbf{u}^{(i)} + \mathbf{u}^{(r)}$. For $y < 0$, we have a transmitted wave $\mathbf{u}^{(t)}$ which is identical to the the total wave field $\mathbf{u}$. The reflected and transmitted waves can be expanded in Fourier series as

$$\mathbf{u}^{(r)}(\mathbf{r}) = \sum_{j=-\infty}^{\infty} \mathbf{B}_j \exp[i(\alpha_j x + \beta_j^{(t)} y)], \quad y > D, \tag{14}$$

$$\mathbf{u}^{(t)}(\mathbf{r}) = \sum_{j=-\infty}^{\infty} \mathbf{C}_j \exp[i(\alpha_j x - \beta_j^{(b)} y)], \quad y < 0, \tag{15}$$

where $\mathbf{B}_j$, $\mathbf{C}_j$ are vector coefficients, and

$$\alpha_j = \alpha_0 + 2\pi j/L, \quad \beta_j^{(t)} = \sqrt{\eta_t - \alpha_j^2}, \quad \beta_j^{(b)} = \sqrt{\eta_b - \alpha_j^2}, \quad \eta_b = k_0^2 \varepsilon_b \mu_b - \gamma_0^2.$$

For a given incident wave, our objective is to calculate the coefficients $\{\mathbf{B}_j, \mathbf{C}_j\}$.

If we write down the vectors $\mathbf{A}$, $\mathbf{B}_j$ and $\mathbf{C}_j$ as

$$\mathbf{A} = \begin{bmatrix} A^{(e)} \\ A^{(h)} \end{bmatrix}, \quad \mathbf{B}_j = \begin{bmatrix} B_j^{(e)} \\ B_j^{(h)} \end{bmatrix}, \quad \mathbf{C}_j = \begin{bmatrix} C_j^{(e)} \\ C_j^{(h)} \end{bmatrix},$$

and normalize the incident wave by

$$\frac{\beta_0^{(t)}}{\eta_t} \left(\varepsilon_t |A^{(e)}|^2 + \mu_t |A^{(h)}|^2 \right) = 1, \tag{16}$$

then the relative power carried by the j-th reflected and transmitted plane waves are

$$R_j = \frac{\mathrm{Re}(\beta_j^{(t)})}{\eta_t} \left(\varepsilon_t |B_j^{(e)}|^2 + \mu_t |B_j^{(h)}|^2 \right), \tag{17}$$

$$T_j = \frac{\mathrm{Re}(\beta_j^{(b)})}{\eta_b} \left(\varepsilon_b |C_j^{(e)}|^2 + \mu_b |C_j^{(h)}|^2 \right). \tag{18}$$

The total power transmittance is $T = \sum T_j$. For a lossless structure, the energy-balance theorem gives $\sum (R_j + T_j) = 1$.

2.C. Boundary conditions

The diffraction problem can be formulated on the rectangular domain S given by $0 < x < L$ and $0 < y < D$. The quasi-periodic condition (13) gives rise to

$$\mathbf{u}(L, y) = \exp(i\alpha_0 L)\, \mathbf{u}(0, y), \quad \partial_x \mathbf{u}(L^+, y) = \exp(i\alpha_0 L)\, \partial_x \mathbf{u}(0^+, y). \tag{19}$$

Meanwhile, we can define two operators $\mathcal{S}_b$ and $\mathcal{S}_t$, and write down exact boundary conditions at $y = 0^-$ and $y = D^+$ as

$$\partial_y \mathbf{u} = \mathcal{S}_b \mathbf{u}, \qquad y = 0^-, \tag{20}$$

$$\partial_y \mathbf{u} = \mathcal{S}_t \mathbf{u} - 2\mathcal{S}_t \mathbf{u}^{(i)}, \quad y = D^+. \tag{21}$$

The governing equations (3) and (4) and the extra conditions (19), (20) and (21) comprise a boundary value problem on the rectangle S.

To define $\mathcal{S}_b$, we first define a linear operator $\mathcal{S}_{bb}$ satisfying

$$\mathcal{S}_{bb} \exp(i\alpha_j x) = -i\beta_j^{(b)} \exp(i\alpha_j x), \quad j = 0, \pm 1, \pm 2, ... \tag{22}$$

Since it is linear, we have

$$\mathcal{S}_{bb} \left[\sum_{j=-\infty}^{\infty} c_j \exp(i\alpha_j x) \right] = -i \sum_{j=-\infty}^{\infty} c_j \beta_j^{(b)} \exp(i\alpha_j x).$$

Therefore, for the scalar function given by

$$\phi(\mathbf{r}) = \sum_{j=-\infty}^{\infty} c_j \exp[i(\alpha_j x - \beta_j^{(b)} y)], \quad y < 0$$

we have $\partial_y \phi = \mathcal{S}_{bb}\, \phi$ at $y = 0^-$. Since each component of $\mathbf{u} = \mathbf{u}^{(t)}$ for $y < 0$ has the same expansion as ϕ above, we have

$$\mathcal{S}_b = \begin{bmatrix} \mathcal{S}_{bb} & 0 \\ 0 & \mathcal{S}_{bb} \end{bmatrix}. \tag{23}$$

Similarly, $\mathcal{S}_t$ is a 2×2 matrix operator whose diagonal entries are $\mathcal{S}_{tt}$, where $\mathcal{S}_{tt}$ maps $\exp(i\alpha_j x)$ to $i\beta_j^{(t)} \exp(i\alpha_j x)$.

In practice, if $x \in (0, L)$ is discretized by N points, the operators $\mathcal{S}_b$ and $\mathcal{S}_t$ are approximated by $(2N) \times (2N)$ matrices. For $\mathcal{S}_{bb}$, Eq. (22) gives us an $N \times N$ matrix, if we retain N different values of j, and consider $\exp(i\alpha_j x)$ (at the N discrete points of x) as an eigenvector and $-i\beta_j^{(b)}$ as the corresponding eigenvalue. The integer j is chosen to satisfy $-N/2 \le j < N/2$ or $-(N-1)/2 \le j \le (N-1)/2$ for an even or odd N, respectively. The matrix $\mathcal{S}_{bb}$ can be calculated directly from its definition using $O(N^3)$ operations. If the Fast Fourier Transform algorithm is used, the required number of operations is only $O(N^2 \log_2 N)$.

3. Operator marching scheme

In previous work [14–16], we developed an operator marching scheme for scalar 2D problems where the governing equations are (5) or (6). For the vector problem considered in this paper, the main steps of the operator marching scheme remain the same, but a new treatment is needed for operators passing through material interfaces.

As in [16], we divide the rectangular domain $S = \{(x, y) \mid 0 < x < L,\ 0 < y < D\}$ into a number of cells as shown in Fig. 1. The cells Ω_1, Ω_2, ..., Ω_m are separated by the curves

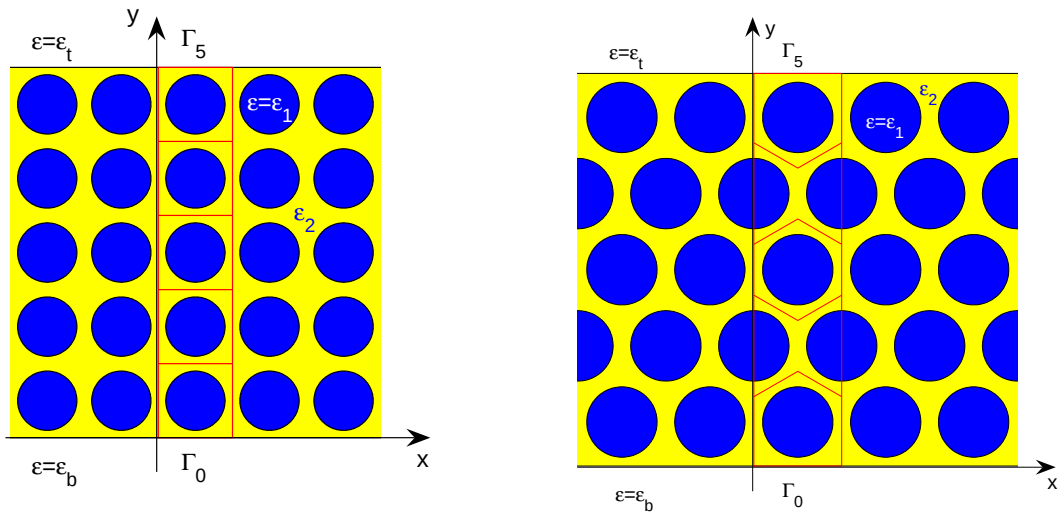

Fig. 1. Five arrays of circular cylinders in a square or triangular lattice. The domain S covering one period of the structure is divided into cells Ω_j for $j = 1$, 2, ..., 5.

Γ_j for $0 \le j \le m$, and bounded by two vertical lines at $x = 0$ and $x = L$. More precisely, the j-th cell Ω_j is bounded by Γ_{j-1}, Γ_j and two vertical line segments at $x = 0$ and $x = L$. In particular, Γ_0 and Γ_m are horizontal line segments at $y = 0$ and $y = D$, respectively. For cylinders on a triangular lattice, the curve Γ_j (for $1 \le j < m$) consists of two edges of the hexagon unit cells. At each point on the curve Γ_j, we assume ν is the upward normal unit vector. On each curve Γ_j, we define operators $\mathcal{Q}_j^{\pm}$ and $\mathcal{Y}_j$ satisfying

$$\mathcal{Q}_j^+ \mathbf{u}_j = \partial_\nu \mathbf{u}_j^+, \quad \mathcal{Q}_j^- \mathbf{u}_j = \partial_\nu \mathbf{u}_j^-, \quad \mathcal{Y}_j \mathbf{u}_j = \mathbf{u}_0, \tag{24}$$

where $\mathbf{u}$ is any solution satisfying the governing equations (3) and (4), the quasi-periodic condition (19) and the radiation condition (20), $\mathbf{u}_j$ denotes $\mathbf{u}$ on Γ_j, and $\partial_\nu \mathbf{u}_j^+$ denotes $\partial_\nu \mathbf{u}$ evaluated on Γ_j^+, etc. We have defined two operators $\mathcal{Q}_j^+$ and $\mathcal{Q}_j^-$ based on the upper and

lower limits toward Γ_j. If the material parameters $\varepsilon(\mathbf{r})$ and $\mu(\mathbf{r})$ are not continuous across Γ_j, then the normal derivative $\partial_\nu \mathbf{u}$ is not continuous there. The main steps of the operator marching scheme are:

1. initialize $\mathcal{Q}_0^-$ and $\mathcal{Y}_0$ from boundary condition (20) and the definition of $\mathcal{Y}_0$, i.e., $\mathcal{Q}_0^- = \mathcal{S}_b$ and $\mathcal{Y}_0 = I$, where I is the identity operator (matrix);

2. calculate $\mathcal{Q}_0^+$ from $\mathcal{Q}_0^-$;

3. for $j = 1, 2, \ldots, m$,

   (a) calculate $\mathcal{Q}_j^-$ and $\mathcal{Y}_j$ from $\mathcal{Q}_{j-1}^+$ and $\mathcal{Y}_{j-1}$,

   (b) calculate $\mathcal{Q}_j^+$ from $\mathcal{Q}_j^-$;

4. solve $\mathbf{u}$ at $y = D$ from boundary condition (21), i.e., $(\mathcal{Q}_m^+ - \mathcal{S}_t)\mathbf{u}_m = -2\mathcal{S}_t \mathbf{u}^{(i)}|_{y=D^+}$;

5. calculate the reflected wave by subtraction: $\mathbf{u}^{(r)}|_{y=D^+} = \mathbf{u}_m - \mathbf{u}^{(i)}|_{y=D^+}$, and the transmitted wave by $\mathbf{u}^{(t)}|_{y=0^-} = \mathbf{u}_0 = \mathcal{Y}_m \mathbf{u}_m$.

Step 3(a) is the main step that marches the operators from Γ_{j-1} to Γ_j, and it is identical to the scalar version presented in [14, 16]. It relies on the operator $\mathcal{M}$ (the reduced DtN map) satisfying

$$\mathcal{M} \begin{bmatrix} \mathbf{u}_{j-1} \\ \mathbf{u}_j \end{bmatrix} = \begin{bmatrix} \mathcal{M}_{11} & \mathcal{M}_{12} \\ \mathcal{M}_{21} & \mathcal{M}_{22} \end{bmatrix} \begin{bmatrix} \mathbf{u}_{j-1} \\ \mathbf{u}_j \end{bmatrix} = \begin{bmatrix} \partial_\nu \mathbf{u}_{j-1}^+ \\ \partial_\nu \mathbf{u}_j^- \end{bmatrix}, \tag{25}$$

where $\mathbf{u}$ is any solution of (3), (4) and (19). For cells containing circular cylinders, we will describe an efficient method for computing $\mathcal{M}$ in Section 4. Using the 2×2 blocks of $\mathcal{M}$, we have

$$\mathcal{Q}_j^- = \mathcal{M}_{22} + \mathcal{M}_{21}(\mathcal{Q}_{j-1}^+ - \mathcal{M}_{11})^{-1}\mathcal{M}_{12}, \tag{26}$$

$$\mathcal{Y}_j = \mathcal{Y}_{j-1}(\mathcal{Q}_{j-1}^+ - \mathcal{M}_{11})^{-1}\mathcal{M}_{12}. \tag{27}$$

Step 2 and Step 3(b) are related to the interface conditions, that is, the continuity of $\mathbf{u}$ and the two terms given in (8). Let $\varepsilon^\pm$ and $\mu^\pm$ (thus $\eta^\pm$) be the upper and lower limits of these physical parameters toward the curve Γ_j, then the continuity conditions give rise to

$$\mathcal{Q}_j^+ = \begin{bmatrix} t_1 & 0 \\ 0 & t_2 \end{bmatrix} \mathcal{Q}_j^- + \begin{bmatrix} 0 & t_3\,\partial_\tau \\ t_4\,\partial_\tau & 0 \end{bmatrix}, \tag{28}$$

where t_1, t_2, t_3 and t_3 are functions on Γ_j given as

$$t_1 = \frac{\varepsilon^-\eta^+}{\varepsilon^+\eta^-}, \quad t_2 = \frac{\mu^-\eta^+}{\mu^+\eta^-}, \quad t_3 = \frac{\gamma_0(\eta^+ - \eta^-)}{k_0\eta^-\varepsilon^+}, \quad t_4 = -\frac{\gamma_0(\eta^+ - \eta^-)}{k_0\eta^-\mu^+}.$$

For the special case of $\gamma_0 = 0$, we have $t_3 = t_4 = 0$, $t_1 = \mu^+/\mu^-$ and $t_2 = \varepsilon^+/\varepsilon^-$, which exactly correspond to continuity of $\mu^{-1}E_z$ and $\varepsilon^{-1}\tilde{H}_z$. In general, E_z and $\tilde{H}_z$ are coupled on the interface and the tangential derivative is involved. In the discrete case, if Γ_j is sampled by N points, t_1, t_2, t_3 and t_4 are represented by $N \times N$ diagonal matrices, ∂_τ is represented by an $N \times N$ matrix (the differentiation matrix) depending on how the tangential derivative is approximated. On Γ_0 and Γ_m, the normal derivative is ∂_y, but the tangential derivative is actually $-\partial_x$ due to our definition of unit vector τ in Section 2. Similar to the treatment for $\mathcal{S}_{bb}$, we first evaluate ∂_x on each term of the Fourier series:

$$\partial_x \exp(i\alpha_j x) = i\alpha_j \exp(i\alpha_j x), \quad j = 0, \pm 1, \pm 2, ..., \tag{29}$$

then find a matrix whose eigenvalues are $i\alpha_j$ and eigenvectors are $\exp(i\alpha_j x)$ (as a column vector at the N points of x) for N retained integers j.

4. Dirichlet-to-Neumann map of a unit cell

The marching step in the previous section relies on the operator $\mathcal{M}$ satisfying (25). Since the vertical edges of Ω_j are not involved, we call $\mathcal{M}$ the reduced DtN map of Ω_j. In contrast, the (full) DtN map of Ω_j is the operator Λ that maps $\mathbf{u}$ on $\partial\Omega_j$ to $\partial_\nu \mathbf{u}$ on $\partial\Omega_j$, where $\partial\Omega_j$ is the full boundary of Ω_j consisting of Γ_{j-1}, Γ_j and the two vertical edges. Furthermore, since $\partial\Omega_j$ may contain material interfaces, $\partial_\nu \mathbf{u}$ is evaluated as the interior limit towards the boundary. More specifically, if we choose the upward unit normal vector on Γ_j and Γ_{j-1} as before, and choose the unit vector in the x direction as the normal vector on the vertical edges, then Λ satisfies

$$\Lambda \begin{bmatrix} \mathbf{u}_{j-1} \\ \mathbf{w}_0 \\ \mathbf{w}_1 \\ \mathbf{u}_j \end{bmatrix} = \begin{bmatrix} \Lambda_{11} & \Lambda_{12} & \Lambda_{13} & \Lambda_{14} \\ \Lambda_{21} & \Lambda_{22} & \Lambda_{23} & \Lambda_{24} \\ \Lambda_{31} & \Lambda_{32} & \Lambda_{33} & \Lambda_{34} \\ \Lambda_{41} & \Lambda_{42} & \Lambda_{43} & \Lambda_{44} \end{bmatrix} \begin{bmatrix} \mathbf{u}_{j-1} \\ \mathbf{w}_0 \\ \mathbf{w}_1 \\ \mathbf{u}_j \end{bmatrix} = \begin{bmatrix} \partial_\nu \mathbf{u}_{j-1}^+ \\ \partial_x \mathbf{w}_0^+ \\ \partial_x \mathbf{w}_1^- \\ \partial_\nu \mathbf{u}_j^- \end{bmatrix}, \tag{30}$$

where $\mathbf{u}_{j-1}$, $\mathbf{u}_j$, $\mathbf{w}_0$ and $\mathbf{w}_1$ denote $\mathbf{u}$ on Γ_{j-1}, Γ_j and the vertical edges at $x = 0$ and $x = L$, respectively, $\partial_\nu \mathbf{u}_{j-1}^+$, $\partial_\nu \mathbf{u}_j^-$, $\partial_x \mathbf{w}_0^+$ and $\partial_x \mathbf{w}_1^-$ denote the interior limits of $\partial_\nu \mathbf{u}$ on the four edges. It turns out that $\mathcal{M}$ can be obtained from Λ when the quasi-periodic condition (19) is incorporated. For unit cells that contain circular cylinders such as dielectric rods or air-holes, we have previously used cylindrical waves to construct matrix approximations of Λ for scalar 2D problems [14,16]. In the following, we extend the construction to vector problems based on vector cylindrical wave expansions. For non-circular cylinders, a boundary integral equation method was previously used to construct Λ for scalar 2D problems [18]. The extension of that method to vector problems will be presented in our future work.

Consider a unit cell Ω that contains a circular cylinder of radius a and a homogeneous medium surrounding the cylinder as shown in Fig. 2. The relative permittivity and perme-

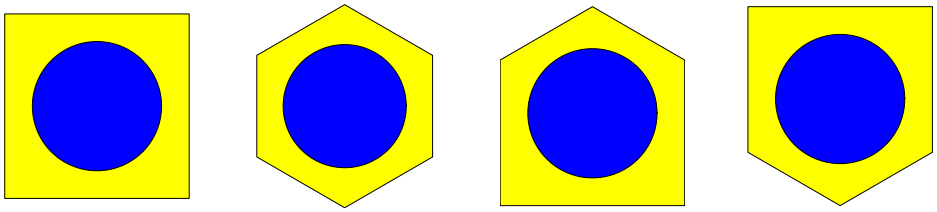

Fig. 2. Square, hexagon and special unit cells each containing one circular cylinder.

ability of the cylinder and the surrounding medium are $\{\varepsilon_1, \mu_1\}$ and $\{\varepsilon_2, \mu_2\}$, respectively. Since the governing equations are reduced to Helmholtz equation (7) in any homogeneous medium, the general solution in Ω can be written as

$$\mathbf{u}(\mathbf{r}) = \begin{cases} \sum\limits_{j=-\infty}^{\infty} \mathbf{a}_j J_j(\rho_1 r)\, e^{ij\theta}, & r < a \\ \sum\limits_{j=-\infty}^{\infty} \left[\mathbf{b}_j J_j(\rho_2 r) + \mathbf{c}_j H_j^{(1)}(\rho_2 r)\right] e^{ij\theta}, & r > a, \end{cases} \tag{31}$$

where $\{r, \theta\}$ is a polar coordinate system with the origin at the center of the cylinder,

$$\rho_1 = \sqrt{\eta_1} = \sqrt{k_0^2 \varepsilon_1 \mu_1 - \gamma_0^2}, \quad \rho_2 = \sqrt{\eta_2} = \sqrt{k_0^2 \varepsilon_2 \mu_2 - \gamma_0^2},$$

$\mathbf{a}_j$, $\mathbf{b}_j$ and $\mathbf{c}_j$ are vectors of length two. From the continuity of $\mathbf{u}$ at $r = a$, we have

$$J_j(\rho_1 a)\, \mathbf{a}_j = J_j(\rho_2 a)\, \mathbf{b}_j + H_j^{(1)}(\rho_2 a)\, \mathbf{c}_j. \tag{32}$$

We also need the continuity of the two terms given in (8). On the boundary of the cylinder, i.e., at $r = a$, the normal derivative becomes ∂_r and the tangential derivative becomes $a^{-1}\partial_\theta$. This gives rise to

$$\mathbf{F}_1\, \mathbf{a}_j = \mathbf{F}_2\, \mathbf{b}_j + \mathbf{F}_3\, \mathbf{c}_j, \tag{33}$$

where $\mathbf{F}_1$, $\mathbf{F}_2$ and $\mathbf{F}_3$ are 2×2 matrices. More precisely,

$$\mathbf{F}_2 = \begin{bmatrix} \frac{\varepsilon_2}{\rho_2} J_j'(\rho_2 a) & \frac{ij\gamma_0}{k_0 a \rho_2^2} J_j(\rho_2 a) \\ -\frac{ij\gamma_0}{k_0 a \rho_2^2} J_j(\rho_2 a) & \frac{\mu_2}{\rho_2} J_j'(\rho_2 a) \end{bmatrix},$$

$\mathbf{F}_1$ is obtained if we replace $\{\varepsilon_2, \mu_2, \rho_2\}$ by $\{\varepsilon_1, \mu_1, \rho_1\}$ in $\mathbf{F}_2$, and $\mathbf{F}_3$ is obtained if we replace J_j by $H_j^{(1)}$ in $\mathbf{F}_2$. Therefore, $\mathbf{a}_j$ and $\mathbf{c}_j$ can be solved in terms of $\mathbf{b}_j$. We write down the result for $\mathbf{c}_j$ as

$$\mathbf{c}_j = \mathbf{T}_j\, \mathbf{b}_j, \tag{34}$$

where $\mathbf{T}_j$ is a 2×2 matrix that depends on the integer j. The general solution in the unit cell Ω can now be written as

$$\mathbf{u}(\mathbf{r}) = \sum_{j=-\infty}^{\infty} \mathbf{\Phi}_j(\mathbf{r})\, \mathbf{b}_j \tag{35}$$

for a 2×2 matrix function $\mathbf{\Phi}_j$. Outside the cylinder, $\mathbf{\Phi}_j$ is given as

$$\mathbf{\Phi}_j(\mathbf{r}) = e^{ij\theta} \left[J_j(\rho_2 r)\mathbf{I} + H_j^{(1)}(\rho_2 r)\mathbf{T}_j \right], \quad r > a, \tag{36}$$

where $\mathbf{I}$ is the 2×2 identity matrix.

With the the general solution in the unit cell Ω given in (35), we can find a matrix approximation to the DtN map Λ based on the approach first used in [14]. We choose K points on the boundary of Ω, say $\mathbf{r}_l$ for $1 \le l \le K$, and also choose a unit normal vector at each of these points, then truncate (35) to K terms and calculate two $(2K) \times (2K)$ matrices $\mathcal{A}$ and $\mathcal{B}$. The matrix $\mathcal{A}$ can be written in $K \times K$ blocks with each block a 2×2 matrix. The l-th block row consists of $\mathbf{\Phi}_j(\mathbf{x}_l)$ for all retained j. Similarly, the l-th block row of the matrix $\mathcal{B}$ consists of $\partial_\nu \mathbf{\Phi}(\mathbf{r}_l)$ for all j. Then, the DtN map is approximated by $\Lambda = \mathcal{B}\mathcal{A}^{-1}$. The normal derivative of $\mathbf{\Phi}(\mathbf{r})$ is related to the normal derivative of the scalar functions $J_j(\rho_2 r)e^{ij\theta}$ and $H_j^{(1)}(\rho_2 r)e^{ij\theta}$. If ϕ is a function of the radial variable r, we have

$$\partial_\nu[\phi(r)e^{ij\theta}] = \phi'(r)e^{ij\theta}\, \nu \cdot \begin{bmatrix} \cos\theta \\ \sin\theta \end{bmatrix} + \frac{ij\phi(r)e^{ij\theta}}{r}\, \nu \cdot \begin{bmatrix} -\sin\theta \\ \cos\theta \end{bmatrix}.$$

Now we return to the unit cell Ω_j bounded by curves Γ_{j-1}, Γ_j and two vertical edges. In the discrete case, $\mathbf{u}_j$, $\mathbf{u}_{j-1}$, $\mathbf{w}_0$ and $\mathbf{w}_1$ in (30) are column vectors whose lengths are twice the numbers of points on the corresponding edges. To calculate the reduced DtN map $\mathcal{M}$, we assume that the material parameters $\{\varepsilon, \mu\}$ are continuous across the vertical lines at $x = 0$ and $x = L$. Then, $\partial_x \mathbf{w}_0^+$ and $\partial_x \mathbf{w}_1^-$ in (30) become simply $\partial_x \mathbf{w}_0$ and $\partial_x \mathbf{w}_1$. The quasi-periodic condition (19) gives us $\mathbf{w}_1 = \xi \mathbf{w}_0$ and $\partial_x \mathbf{w}_1 = \xi \partial_x \mathbf{w}_0$ for $\xi = \exp(i\alpha_0 L)$. We can use these conditions to eliminate $\mathbf{w}_0$ and $\mathbf{w}_1$ in (30) and find $\mathcal{M}$. The process is identical to the scalar case considered in [16], where an explicit formula is given.

For a triangular lattice, when the rectangular domain S is divided into cells, we also encounter cells that contain two half-cylinders such as shown in Fig. 1(right). Additional examples near the top and bottom boundaries are shown in Fig. 3. If Ω_j is such a cell, we do not calculate its DtN map Λ. Instead, we can find the reduced DtN map $\mathcal{M}$ directly from the reduced DtN map $\mathcal{M}'$ of a regular cell Ω_j' that contains one cylinder. Since the structure is periodic in the x direction, we have a regular cell Ω_j' between the periodic extensions of Γ_{j-1} and Γ_j, and for $x \in (L/2, L)$. Using the quasi-periodic condition between the left half of Ω_j and the right half of Ω_j', we can deduce $\mathcal{M}$ from $\mathcal{M}'$. The details are given in [16].

In the above process for approximating Λ and $\mathcal{M}$, we have grouped E_z and $\tilde{H}_z$ together when $\mathbf{u}$ on the boundary of the cell is evaluated at different points. More precisely, if on

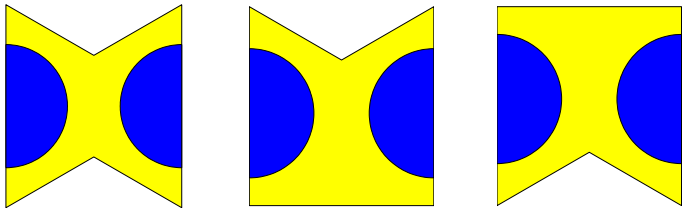

Fig. 3. Unit cells that contain two half-cylinders each.

Γ_{j-1}, we used the points $\mathbf{r}_1$, $\mathbf{r}_2$, ..., then $\mathbf{u}_{j-1}$ in (30) is the column vector

$$\mathbf{u}_{j-1} = [E_z(\mathbf{r}_1),\, \tilde{H}_z(\mathbf{r}_1),\, E_z(\mathbf{r}_2),\, \tilde{H}_z(\mathbf{r}_2),\, ...\,]^T.$$

This is convenient for the construction of Λ and it also has closer analogy with the scalar case studied in [14,16]. However, the matrix $\mathcal{M}$ used in Section 3 corresponds to an ordering where E_z for all points and $\tilde{H}_z$ for all points are grouped in two blocks. For example, the vector $\mathbf{u}_{j-1}$ in (25) should be

$$\mathbf{u}_{j-1} = [E_z(\mathbf{r}_1),\, E_z(\mathbf{r}_2),\, ...,\, \tilde{H}_z(\mathbf{r}_1),\, \tilde{H}_z(\mathbf{r}_2),\, ...\,]^T.$$

Therefore, to find the final version of $\mathcal{M}$, we must carry out a simple permutation.

5. Numerical examples

To illustrate our method, we present a few numerical examples in this section. Only non-magnetic media are involved, therefore the relative permeability is $\mu = 1$. For the first example, we follow the earlier work of Centeno and Felbacq [5] and consider $m = 9$ arrays of circular dielectric cylinders on a triangular lattice. The radius and the dielectric constant of the cylinders are $a = 0.15L$ and $\varepsilon_1 = 8.41$, respectively, where L is the lattice constant. The background medium is air, therefore $\varepsilon_t = \varepsilon_b = \varepsilon_2 = 1$. Centeno and Felbacq [5] studied the dependence of transmittance on the angle of conicity θ_0, but their structure is actually finite with the total of 9×9 cylinders. We study the same problem for infinite and periodic arrays. In Fig. 4, we show the transmittance T as a function of the normalized wavelength $\lambda/L = 2\pi c/(\omega L)$ and the conicity angle θ_0 on a logarithmic scale. The incident wave is E-polarized and its wave vector $\mathbf{k}_0$ is perpendicular to the x axis, that is, $A^{(h)} = 0$ and $\varphi_0 = 270^o$ (thus $\alpha_0 = 0$). Our results agree quite well with those in [5], even though the structures analyzed are not exactly the same. The second example is also adapted from [5]. We consider $m = 9$ arrays of air-holes in an infinite background dielectric medium with $\varepsilon_2 = \varepsilon_t = \varepsilon_b = 12$. The air-holes form a triangular lattice with a lattice constant L, and

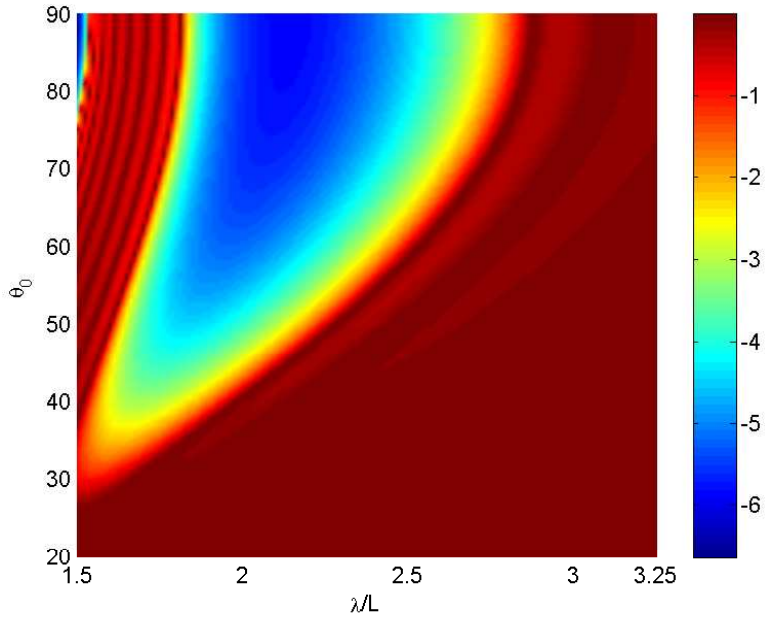

Fig. 4. Logarithm of transmittance T versus normalized wavelength λ/L and conicity angle θ_0 for 9 arrays of dielectric cylinders in a triangular lattice.

the radius of the air-holes is $a = 0.2L$. For H-polarized incident waves with a wave vector perpendicular to the x axis, i.e. $\varphi_0 = 270^o$ and $A^{(e)} = 0$, we obtain the transmittance shown in Fig. 5. Again, we observe good agreement with the result given in [5], even though the authors of [5] considered only 9×9 air-holes.

The third example also consists of $m = 9$ arrays of circular dielectric cylinders arranged as a triangular lattice and surrounded by air, but the cylinders have a larger radius $a = 0.45L$. Since $a > (\sqrt{3}/4)L$, the arrays cannot be separated by planes without intersecting the cylinders. For such a structure involving interpenetrating arrays, existing numerical methods using Fourier series on planes separating the arrays (as in the scattering matrix formalism) have some difficulties. In our previous work [16], we demonstrated the capability of the DtN map method to handle interpenetrating arrays for the pure 2D cases ($\gamma_0 = 0$ or $\theta_0 = 90^o$). For oblique incident waves, our method also works without any difficulty. For this example, we assume that the dielectric constant of the cylinders is $\varepsilon_1 = 11.4$, and consider incident plane waves with the angle of conicity $\theta_0 \approx 64.34^o$ ($\cos\theta_0 = \sqrt{3}/4$) and the angle of incidence $\varphi_0 \approx 286.1^o$ ($\tan\varphi_0 = -2\sqrt{3}$). In Fig. 6, we show the transmission spectra for incident plane waves in both polarizations. An interval of low transmission is observed for both polarizations of the incident field. The transmission spectra also exhibit a few abrupt changes.

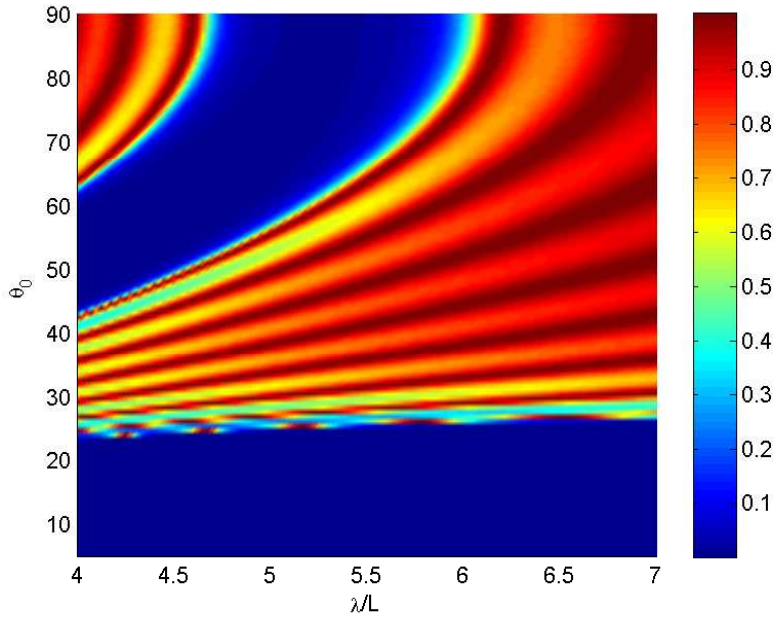

Fig. 5. Transmittance T versus normalized wavelength λ/L and conicity angle θ_0 for 9 arrays of air-holes in a triangular lattice.

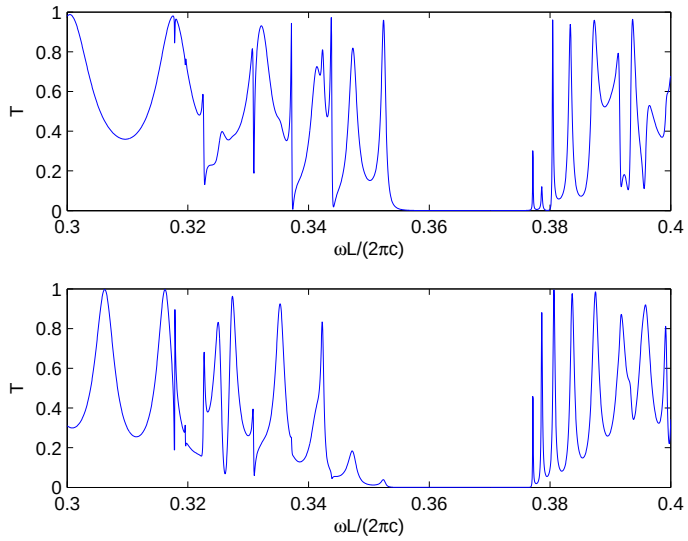

Fig. 6. Transmission spectra of 9 interpenetrating arrays of dielectric cylinders in free space, for oblique incident waves in the E (top) or H (bottom) polarizations (example 3).

The fourth example consists of $m = 7$ interpenetrating arrays of circular air-holes in a dielectric layer with $\varepsilon_2 = 11.4$. The air-holes ($\varepsilon_1 = 1$) are given in a triangular lattice with a lattice constant L, and the radius of the air-holes is $a = 0.45L$. Similar to the case shown in Fig. 1(right), the dielectric layer is given by $0 < y < D$, where $D = [1 + \sqrt{3}(m-1)/2]L = (1 + 3\sqrt{3})L$, and it is surrounded by air, so that $\varepsilon_t = \varepsilon_b = 1$. For the same angles θ_0 and φ_0 used in example 3, we obtain the transmission spectra shown in Fig. 7, where the incident

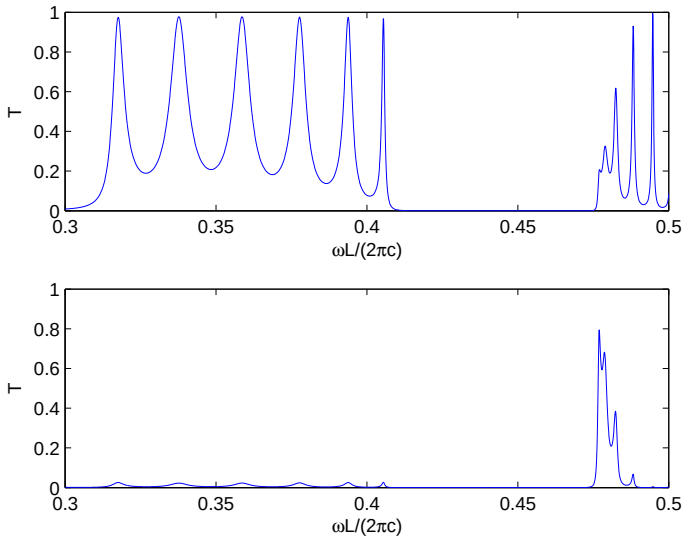

Fig. 7. Transmission spectra of 7 interpenetrating arrays of air-holes in a dielectric layer for oblique incident waves in the E (top) and H (bottom) polarizations (example 4).

wave is either E-polarized ($A^{(h)} = 0$) or H-polarized ($A^{(e)} = 0$). We observe a large interval where transmission is inhibited only if the incident field is H-polarized.

For both examples 3 and 4, we have checked the numerical convergence of our method with respect to the number of collocation points p on each edge of a unit cell. We calculate the relative errors for T_0 or R_0 for a number of frequencies, based on a reference solution obtained with a large p, such as $p = 25$. It appears that the relative errors decrease exponentially as p is increased. For a typical value of $p = 9$, the relative error is usually less than 10^{-3} indicating that 3 or more significant digits are already obtained. Overall, our method is efficient because we only need to manipulate small matrices. For a triangular lattice, when p collocation points are used on each edge of a hexagon unit cell, the DtN map Λ is approximated by a $(12p) \times (12p)$ matrix, the reduced DtN map $\mathcal{M}$ is approximated by a $(8p) \times (8p)$ matrix, and the operators $\mathcal{Q}_j$ and $\mathcal{Y}_j$ are approximated by $(4p) \times (4p)$ matrices (or even smaller matrices

at $y = 0$ and $y = D$). The construction of Λ is the most expensive step of our method, yet it only requires $O((12p)^3)$ operations. Furthermore, both Λ and $\mathcal{M}$ are only calculated for distinct unit cells.

6. Conclusion

In this paper, we presented an efficient method for analyzing diffraction of oblique incident plane waves by periodic arrays of circular cylinders. Our method relies on vector cylindrical wave expansions to approximate the Dirichlet-to-Neumann (DtN) maps for unit cells containing circular cylinders, and it employs an operator marching scheme to solve the problem without further computation in the interiors of the unit cells. Unlike the multipole (scattering matrix) method, our method does not require sophisticated lattice sums techniques and it can handle interpenetrating arrays without any difficulty. Although many numerical and semi-analytic methods are available for conical diffraction problems, our method is highly competitive, since it takes full advantage of the available geometric features.

For ideal two-dimensional problems, where both the structure and the fields are invariant in the z direction, the DtN maps of the unit cells are useful in many computation problems for photonic crystals (PhCs), including band structures [10,11], defect modes [12,13] and PhC devices [17]. With the DtN map constructed in Section 4, we can easily extend these studies to the vector case involving the z dependence of $\exp(i\gamma_0 z)$. In particular, band structure analysis with such a z dependence is relevant to PhC fibers.

Acknowledgments

This research was partially supported by a grant from the Research Grants Council of Hong Kong Special Administrative Region, China (Project No. CityU 102207).

References

1. J. D. Joannopoulos, R. D. Meade, and J. N. Winn, *Photonic Crystals: Molding the Flow of Light*, (Princeton University Press, Princeton, NJ. 1995).
2. A. Taflove and S. C. Hagness, *Computational Electrodynamics: the finite-difference time-domain method*, 2nd ed., (Artech House, 2000).
3. S. Venakides, M. A. Haider, and V. Papanicolaou, "Boundary integral calculations of two-dimensional electromagnetic scattering by photonic crystal Fabry-Perot structures," SIAM Journal on Applied Mathematics **60**, 1686-1706 (2000).
4. D. Pissoort, E. Michielssen, F. Olyslager, and D. De Zutter, "Fast analysis of 2-D electromagnetic crystal devices using a periodic Green function approach," J. Lightwave Technol. **23**, 2294-2308 (2005).

5. E. Centeno, D. Felbacq, "Rigorous vector diffraction of electromagnetic waves by bidimensional photonic crystals," J. Opt. Soc. Am. A **17**, 320-327 (2000).
6. G. H. Smith, L. C. Botten, R. C. McPhedran, and N. A. Nicorovici, "Cylinder gratings in conical incidence with applications to modes of air-cored photonic crystal fibers," Phys. Rev. E **66**, 056604 (2002).
7. G. H. Smith, L. C. Botten, R. C. McPhedran, and N. A. Nicorovici, "Cylinder gratings in conical incidence with applications to woodpile structures," Phys. Rev. E **67**, 056620 (2003).
8. L. C. Botten, T. P. White, A. A. Asatryan, et al., "Bloch mode scattering matrix methods for modeling extended photonic crystal structures. I. Theory," Phys. Rev. E **70**, 056606 (2004).
9. K. Yasumoto, H. Toyama and T. Kushta, "Accurate analysis of two-dimensional electromagnetic scattering from multilayered periodic arrays of circular cylinders using lattice sums technique," IEEE Transactions on Antennas and Propagation **52**, 2603-2611 (2004).
10. J. Yuan and Y. Y. Lu, "Photonic bandgap calculations using Dirichlet-to-Neumann maps," J. Opt. Soc. Am. A **23**, 3217-3222 (2006).
11. J. Yuan and Y. Y. Lu, "Computing photonic band structures by Dirichlet-to-Neumann maps: The triangular lattice," Opt. Commun. **273**, 114-120 (2007).
12. Y. Huang, Y. Y. Lu and S. Li, "Analyzing photonic crystal waveguides by Dirichlet-to-Neumann maps," J. Opt. Soc. Am. B **24**, 2860-2867 (2008).
13. S. Li and Y. Y. Lu, "Computing photonic crystal defect modes by Dirichlet-to-Neumann maps," Opt. Express **15**, 14454-14466 (2007).
14. Y. Huang and Y. Y. Lu, "Scattering from periodic arrays of cylinders by Dirichlet-to-Neumann maps," J. Lightwave Technol. **24**, 3448-3453 (2006).
15. Y. Huang and Y. Y. Lu, "Modeling photonic crystals with complex unit cells by Dirichlet-to-Neumann maps", J. Comput. Math. **25**, 337-349 (2007).
16. Y. Wu and Y. Y. Lu, "Dirichlet-to-Neumann map method for analyzing interpenetrating cylinder arrays in a triangular lattice," J. Opt. Soc. Am. B **25**, 1466-1473 (2008).
17. Z. Hu and Y. Y. Lu, "Efficient analysis of photonic crystal devices by Dirichlet-to-Neumann maps," Opt. Express **16**, 17383-17399 (2008).
18. J. Yuan, Y. Y. Lu, and X. Antoine, "Modeling photonic crystals by boundary integral equations and Dirichlet-to-Neumann maps," J. Comput. Phys. **227**, 4617-4629, (2008).
19. L. Li, "A modal analysis of lamellar diffraction gratings in cornical mountings," J. Mod. Opt. **40**, 553-573 (1993).
20. S. Campbell, L. C. Botten, C. M. De Sterke, and R. C. McPhedran, "Fresnel formulation for multi-element lamellar diffraction gratings in conical mountings," Waves in Random and Complex Media **17**, 455-475 (2007).

21. B. Gralak, R. Pierre, G. Tayeb, and S. Enoch, "Solutions of Maxwell's equations in presence of lamellar gratings including infinitely conducting metal," J. Opt. Soc. Am. A **25**, 3099-3110 (2008).
22. P. Lalanne and G. M. Morris, "Highly improved convergence of the coupled-wave method for TM polarization", J. Opt. Soc. Am. A **13**, 779-784 (1996).
23. L. Li, "Formulation and comparison of two recursive matrix algorithms for modeling layered diffraction gratings", J. Opt. Soc. Am. A **13**, 1024-1035 (1996).
24. E. Popov and B. Bozhkov, "Differential method applied for photonic crystals," Appl. Opt. **39**, 4926-4932 (2000).
25. J. Elschner, R. Hinder, and G. Schmidt, "Finite element solution of conical diffraction problems," Advances in Computational Mathematics **16**, 139-156 (2002).
26. G. Bao Z. M. Chen and H. J. Wu, "Adaptive finite-element method for diffraction gratings", J. Opt. Soc. Am. A **22**, 1106-1114 (2005).
27. A. Pomp, "The integral method for coated gratings – computational cost," J. Mod. Opt. **38**, 109-120 (1991).
28. D. W. Prather, M. S. Mirotznik, and J. N. Mait, "Boundary integral methods applied to the analysis of diffractive optical elements," J. Opt. Soc. Am. A **14**, 34-43 (1997).
29. E. Popov, B. Bozhkov, D. Maystre, and J. Hoose, "Integral method for echelles covered with lossless or absorbing thin dielectric layers," Applied Optics **38**, 47-55 (1999).
30. A. Rathsfeld, G. Schmidt, and B. H. Kleemann, "On a fast integral equation method for diffraction gratings," Communications in Computational Physics **1**, 984-1009 (2006).